HHS Public Access

Author manuscript

Adv Mater. Author manuscript; available in PMC 2019 September 01.

Published in final edited form as:

Adv Mater. 2018 September ; 30(39): e1802762. doi:10.1002/adma.201802762.

Non-destructive Real-Time Monitoring of Enhanced Stem Cell Differentiation using a Graphene-Au Hybrid Nanoelectrode Array

Jin-Ho Lee[1,2], **Hye Kyu Choi**[2], **Letao Yang**[1], **Sy-Tsong Dean Chueng**[1], **Jeong-Woo Choi**[2], and **Ki-Bum Lee**[1,3]

[1]Department of Chemistry Department of Chemistry and Chemical Biology Institute for Advanced Materials, Devices and Nanotechnology (IAMDN), Rutgers University, Piscataway, NJ 08854, USA, kblee@rutgers.edu, Tel: +1-848-445-2081

[2]Department of Chemical and Biomolecular Engineering, Sogang University, Seoul, 04107, Korea, jwchoi@sogang.ac.kr, Tel: +82-2-705-8480

[3]College of Pharmacy, Kyung Hee University, 26 Kyungheedae-ro, Dongdaemun-gu, Seoul 02447, Korea

Abstract

Stem cells have attracted increasing research interest in the field of regenerative medicine because of their unique ability to differentiate into multiple cell lineages. However, controlling stem cell differentiation efficiently and improving the current destructive characterization methods for monitoring stem cell differentiation are the critical issues. To this end, we developed multifunctional graphene-gold (Au) hybrid nanoelectrode arrays (NEAs) to i) investigate the effects of combinatorial physicochemical cues on stem cell differentiation, ii) enhance stem cell differentiation efficiency through biophysical cues, and iii) characterize stem cell differentiation in a non-destructive real-time manner. Through the synergistic effects of physiochemical properties of graphene and biophysical cues from nanoarrays, our graphene-Au hybrid NEAs facilitated highly enhanced cell adhesion and spreading behaviors. In addition, by varying the dimensions of the graphene-Au hybrid NEAs, we showed improved stem cell differentiation efficiency, resulting from the increased focal adhesion signal. Furthermore, we utilized our graphene-Au hybrid NEAs to monitor osteogenic differentiation of stem cells electrochemically in a non-destructive real-time manner. Collectively, we believe our unique multifunctional graphene-Au hybrid NEAs can significantly advance stem cell-based biomedical applications.

Graphical Abstract

SUPPORTING INFORMATION

Supporting Information is available from the Wiley Online Library or the author.

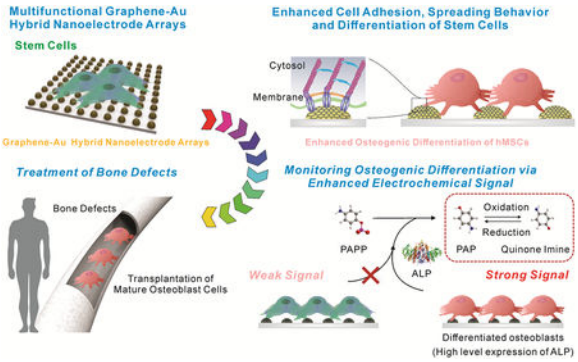

We developed a multifunctional graphene-Au hybrid Nanoelectrode Arrays (NEAs). Owing to the combinatory effect of graphene and biophysical cues, our graphene-Au hybrid NEAs showed highly improved cell adhesion and spreading behavior which resulted in an enhanced osteogenesis. Additionally, improved electrochemical sensitivity allowed the monitoring of osteogenic differentiation in a non-destructive real-time manner.

Keywords

Graphene-Au Hybrid Nanoelectrode Array; Stem cell differentiation; Osteogenesis from stem cells; Non-destructive Real-time detection; Biosensing

Stem cell-based regenerative medicine has attracted increasing attention in the area of biomaterial science and tissue engineering. For example, stem cell-based approaches hold great potential in treating many musculoskeletal diseases and injuries.[1] However, the ability to differentiate stem cells into specific cell types of interest (e.g. bones, cartilages, and muscles) in a highly selective and efficient manner, and the development of non-destructive, real-time characterization methods to assay stem cell differentiation are crucial in harnessing the full potential of stem cell-based biomaterial applications.[2, 3]

Conventional methods to control stem cell differentiation using soluble cues such as growth factors, cytokines, and small organic molecules have shown limited success in achieving high differentiation specificity and efficiency. Recent findings show that biophysical (or insoluble) cues also play a critical role in guiding stem cell differentiation.[4, 5, 6, 7, 8, 9] Encompassing nanotopographical and mechanical properties of microenvironment, biophysical cues are known to be effective regulators of cytoskeletal dynamics and downstream gene expression [e.g., extracellular matrix (ECM)-integrin-cytoskeleton signaling transduction], thereby modulating stem cell behaviors such as proliferation, migration, and differentiation.[4] Therefore, there is a clear need to develop a novel method to identify the optimal biophysical cues in a combinatorial way for guiding stem cell differentiation into specific cell lineages. These identified biophysical cues can be further combined with defined soluble factors to bring synergistic differentiation conditions, which will facilitate the advancement of stem cell-based applications such as the regeneration of certain types of damaged tissues/organs of patients.

Another critical challenge is to avoid the possible tumorigenicity associated with stem cell therapy.[3] To this end, the precise characterization of stem cell differentiation at each stage using biomarkers in a non-destructive manner while maintaining high cell viability is essential. Conventional methods for analyzing the biological characteristics of differentiated cells such as fluorescence-based methods [e.g., immunostaining and fluorescence-activated cell sorting (FACS)] and analysis of the expression of biomarkers (DNAs/RNAs/proteins) [e.g., polymerase chain reaction (PCR) and western blot] are commonly used; however, these methods typically require destructive steps such as cell fixation or cell lysis, which prevent the subsequent applications of the characterized cells.[10] Therefore, the development of novel methods that can effectively monitor stem cell differentiation dynamics in a non-destructive manner is urgent.

Addressing the challenges above, herein we demonstrate the versatility of our novel graphene-Au hybrid nanoelectrode combinatorial arrays (**graphene-Au hybrid NEAs**) to: i) investigate the combinatorial effects of physicochemical cues on stem cell differentiation [Figure. 1a], ii) identify the optimal biophysical cues to enhance stem cell osteogenic differentiation [Figure. 1b], and iii) non-destructively monitor the dynamic status of stem cell differentiation in a real-time manner [Figure. 1b]. The osteogenesis of human mesenchymal stem cell (hMSC) was selected as a proof-of-concept model for this study.[11]

Typically, our multifunctional graphene-Au hybrid NEAs are fabricated via laser interference lithography (LIL) and physical vapor deposition (PVD) methods. We tested different variables of the graphene-Au hybrid NEAs such as pitch and pattern sizes to identify the optimal biophysical cues for osteogenic differentiation of stem cells. Reduced graphene oxide (rGO) was chemically attached and modified to the surface of Au NEAs to enhance the adhesion and spreading behaviors of the stem cells. Since the focal adhesion and the rearrangement of the cytoskeleton is critical in determining cell behaviors, we hypothesized that our developed multifunctional graphene-Au hybrid NEAs could regulate stem cell fate through physicochemical and biophysical cues [Figure 1b].[4, 12] Also, the unique physicochemical properties of rGO can promote cell adhesion and spreading behaviors on the NEAs without comprising its electrochemical property [Figure 1a].[6, 13, 14] Taking advantage of the high electron transfer rate based from 3D nanostructures [Figure $1c_1$], our graphene-Au hybrid NEAs has the potential to be utilized as an excellent electrochemical sensing platform, enabling scientists to characterize the subtle changes of biomarker expression [alkaline phosphatase (**ALP**, a pre-osteogenic marker)] [Figure $1c_2$]. Collectively, our graphene-Au hybrid NEAs, as designed, could have the ability to enhance and monitor osteogenic differentiation of stem cell, hMSCs, in a non-destructive real-time manner.

As biophysical cues (e.g. nanotopography, elastic module, pattern dimension, and geometry) have been shown to enhance stem cell differentiation by regulating cell adhesion and spreading behaviors,[4, 12, 15] we generated a combinatorial graphene-Au hybrid NEA as illustrated in Figure. 2a. To identify the optimized biophysical cues for stem cell osteogenesis, four different pitch sizes (400, 800, 1,200, and 1,600 nm) of large-scale (1×1 cm^2) homogeneous photoresist (PR) nano-hole pattern arrays were generated through the LIL technique on an indium tin oxide (ITO) substrate [Figure. 2b and Figure. S1].[16] We

then deposited 15 nm of chromium (Cr) as an adhesion layer and 90 nm of gold (Au) as a conducting layer via PVD onto the PR nano-hole array. The PR was sequentially removed to obtain the four different sized homogenous Au NEAs with controlled width (200, 400, 600, and 800 nm), gap (200, 400, 600, and 800 nm), and height (105 nm) parameters [Figure. 2c and Figure. S1]. The pitch size and height of Au NEAs were carefully designed not only to isolate cells from the underlying flat substrate by disrupting integrin-substratum interactions but also to reconstitute integrin clustering on NEAs by controlling the width and gap of physical dimensions to the submicron range.[4, 17] In parallel, graphene oxide (GO) sheets were synthesized through a modified Hummers' method with a pre-oxidation step. For the sufficient coating of GO onto the Au NEAs surface, the size of GO sheet was adjusted to below 200 nm by an additional filtration process to obtain smaller GO nanosheets. To characterize the as-prepared GO sheets, transmission electron microscopy (TEM) measurement was performed [Figure. 2d]. We also analyzed the size distribution of GO by both dynamic light scattering (DLS) measurement and TEM images. The size distribution of the GO sheets ranged from 37.84 nm to 190.10 nm with an average size of 63.75 ± 24.63 nm in DLS analysis, [Figure. 2e] and 100.4 ± 39.4 nm in TEM images. [Figure. S2] Both results clearly demonstrates the selected size distribution of GO less than 200 nm after filtration process. Further, as-prepared GO sheets were functionalized onto the surface of Au NEAs through electrostatic interactions by utilizing a chemical linker (cysteamine hydrochloride: C_2H_7NS). Finally, GO sheets are chemically reduced by hydrazine monohydrate ($NH_2NH_2 \cdot H_2O$) solution to obtain the graphene-Au hybrid NEAs. Due to the unique physicochemical structure of atomic thin layered rGO, we conducted Raman spectroscopy to properly validate the rGO coating on the Au NEAs. As expected, Raman transition band at the location of the distinct D (1,350 cm^{-1}) and G (1,600 cm^{-1}) band of reduced GO (rGO) were observed from both rGO (functionalized on bare Au substrate) and graphene-Au hybrid NEAs, which meets previously reported literatures.[18] The reduction of GO to rGO on graphene-Au hybrid NEAs was also validated by the comparison of Raman intensity ratio between D and G band (I_D/I_G) before and after the reduction process. As clearly shown in figure S3, the I_D/I_G ratio increases from 0.90 to 1.22 as GO reduces to rGO, respectively [Figure. S3].[19] Moreover, a remarkably strong Raman transition band of rGO [Figure. 2f] as well as intense, homogenously distributed Raman transition (distinct G band, 1,600 cm^{-1}, of rGO) signals over a large scan area (100 × 100 spots per 100 × 100 μm^2) [Figure. 2g] were observed from the graphene-Au hybrid NEAs owing to the surface-enhanced Raman scattering effect caused by the Au nanodots.

Knowing cell adhesion/spreading behaviors and the elongated cell morphology can promote stem cell osteogenesis,[4, 5, 6, 20] we hypothesized that our graphene-Au hybrid NEAs could enhance osteogenic differentiation of hMSCs through the unique physiochemical cues from our graphene-Au hybrid NEAs [Figure. 3a]. To test this hypothesis, hMSCs, cultured on tissue culture plate (TCP), Au NEAs, and graphene-Au hybrid NEAs for 4 hrs, were fixed for 10 mins and characterized using Hoechst to stain their nucleus and fluorescent dye (Alexa Fluor 633) to stain their cytoskeleton (F-actin). No notable difference was observed for the number of cells adhered on the TCP and Au NEAs; however, the presence of nanotopographical cues in Au NEAs allowed the cells to spread more extensively and homogeneously, compared to the experimental condition of TCP. Moreover, due to the

unique physiochemical property of graphene (e.g., amphiphilic and nanoscopic properties), both the number and the size of adhered cells significantly increased on the graphene-Au hybrid NEAs, compared to that of TCP and Au NEA conditions [Figure. 3b]. We quantitatively analyzed the number and the size of adhered cells using five 1,320 × 1,320 μm^2 area-fluorescent images, randomly selected from each condition. The average number of cells were 83.0 ± 40.3, 92.6 ± 15.2, and 149.4 ± 46.7, and the average size of the cells were 2,955.9 ± 584.9, 3,457.9 ± 298.9, and 3,890.8 ± 272.6 μm^2, corresponding to the TCP, Au NEA, and graphene-Au hybrid NEA conditions respectively [Figure. 3c].

To examine further, hMSCs that were grown on graphene-Au hybrid NEAs for a day were treated with differentiation induction medium (osteogenic medium: OM) to study the optimal biophysical cues on osteogenesis. All the cells treated with OM showed the expression of ALP (pre-osteogenic marker) regardless of substrate types used; however, hMSCs on the graphene-Au hybrid NEAs with 400 nm sized (in diameter) nanodots among the 4 different conditions (pattern sizes; 200, 400, 600, and 800 nm) [Figure. 3d] showed the highest ALP activity on day 14 (D14), supporting the synergistic effect of the biophysical cues combined with the soluble cues [Figure. 3d].[21] We also conducted real-time quantitative PCR on D14 to detect biomarkers of osteoblast lineage such as runt-related transcription factor 2 (RUNX2) and focal adhesion kinase/protein tyrosine kinase 2 (FAK/PTK2) genes to investigate the effects of each nanopattern on osteogenic differentiation.[9] It is known that appropriate biophysical cues, such as nanotopography and pattern dimension, can enhance the formation of integrin-mediated small clustering adhesion sites termed focal adhesions (FAs),[4] which affect cell spreading behavior and facilitate lamellipodial protrusions.[22] Moreover, the formation of FA complexes stimulates multiple intracellular signaling cascades such as the mitogen-activated protein kinase-extracellular signal-regulated kinase (MAPK-ERK) 1/2 pathway that activates RUNX2, resulting in increased osteogenic differentiation.[23] We also confirmed the clear co-related upregulation between the FAK/PTK2 gene and the RUNX2 gene in our tested graphene-Au hybrid NEAs. In particular, as predicted from the ALP activity assay, the level of molecular markers for both osteoblast lineage (RUNX2) and the focal adhesion kinase (FAK/PTK2) gene also showed the highest expression from the 400 nm sized graphene-Au hybrid NEA condition [Figure. 3e]. This indicates that early osteogenic differentiation can be synergistically enhanced through the proper choice of biophysical cues. Immunostaining also showed the highest coverage and expression of osteocalcin from the 400 nm diameter graphene-Au hybrid NEA condition [Figure. 3f].[8, 9, 21] From the Alizarin red S assay, which checks the level of calcification, one of the most significant indicators for bone regeneration, we also observed cells grown on the 400 nm sized graphene-Au hybrid NEAs showed the highest level of calcification [Figure. 3g].[8] Collectively, the above results support our hypothesis that appropriate biophysical cues of our graphene-Au hybrid NEAs can enhance the formation of mature osteoblasts, which is highly desirable for further *in vivo* applications such as treating bone defects.

Furthermore, we developed our graphene-Au hybrid NEAs (400 nm sized graphene-Au hybrid NEAs, hereafter termed graphene-Au hybrid NEAs) as a non-destructive real-time electrochemical sensing platform to monitor stem cell differentiation [Figure. 4]. Since most of the electrochemical reaction happens in proximity to the electrode surface, the surface

dimension and its modification are crucial for the performance of electrochemical sensing. For this purpose, nanomaterial (Au and carbon)-based electrochemical sensors have been developed owing to their unique physicochemical properties including high conductivity, inertness, and biocompatibility.[13, 14, 24] Additionally, the higher surface-to-volume ratio of the nanostructures can also increase the electrochemical sensing performance.[14, 25] We conducted cyclic voltammograms (CV) by using 1mM of ferrocyanide $[Fe(CN)_6]^{4-}$ as a well-defined electroactive (reduction and oxidation: redox) chemical in phosphate buffered saline (PBS, pH 7.4) at a scan rate of 50 mV/s to measure the electrochemical signal from each electrode (bare ITO, Au NEAs, and graphene-Au hybrid NEAs) [Figure. 4b]. As expected, there was no observable faradaic current on the bare ITO substrate. However, a large current, intense oxidation and reduction peak (I_{PA} and I_{PC}) were observed on the both rGO-ITO and Au NEAs. In particular, graphene-Au hybrid NEAs displayed a narrower and higher I_{PA} and I_{PC} due to the better electron transfer rate and faster diffusion of oxidant/reductant obtained through the additive effect obtained by both rGO and Au NEAs.[13, 14] We also validated the electrochemical performance based on the reduction degree of rGO. As shown in figure S4, no observable faradaic current on the GO coated ITO substrate, which could be due to the impeded electron transfer. However, an intense I_{PA} and I_{PC} were observed after reduction process. The signal was kept increased and saturated after 9 hr reduction.[26]

We then utilized our graphene-Au hybrid NEAs to examine an ALP-based enzymatic reaction in a cell-free configuration as an initial proof-of-concept before monitoring the osteogenic differentiation process of hMSCs. The expression of ALP, a major biomarker for osteogenesis,[27] arose sequentially during the osteogenic differentiation. As shown in figure 4a, ALP catalytically hydrolyzed the P-aminophenyl phosphate (PAPP) to produce electroactive p-aminophenol (PAP), and the redox reaction between PAP and Quinone imine (QI) was monitored through cyclic voltammogram by utilizing graphene-Au hybrid NEAs as a sensing platform [Figure. 4a]. Before the addition of ALP, no observable redox peak was monitored for the PAPP (1mM) dissolved PBS solution. However, observable redox peaks were obtained 30 minutes after the addition of ALP into the solution, at approximately 0.2 V for the oxidation (I_{PA}) potential and 0.01 V for the reduction (I_{PC}) potential [Figure. 4c]. Comparably, no observable oxidation signal (I_{PA}) was obtained on the bare ITO substrate for neither condition: absence or presence of ALP. Particularly, a remarkable oxidation peak was observed only at the graphene-Au hybrid NEAs when ALP was presented, which proved its excellent sensitivity for the electrochemical detection of PAP resulted from ALP catalytic reaction [Figure. 4d]. To support these results, we also calculated the HOMO and LUMO of PAP molecule and compare it to the band edge positions of rGO, Au and ITO that are reported in literature.[28] When no voltage bias is applied, rGO has less barrier to receive electron from PAP molecules, which leads to the oxidation of PAP into QI. [Figure. S5] In addition, Graphene-Au hybrid NEAs with increased electrode surface area could also increase electron transfer rate by facilitating the electron and mass diffusion. Such improvements can be directly supported by the increased I_{PA} shown in figure 4c and narrowed voltage difference between I_{PA} and I_{PC} shown in figure 4b. Moreover, graphene-Au hybrid NEAs showed good linearity ($R^2 = 0.98$) at different concentrations (range from 0.1 to 10 units/mL) of ALP with a limit of detection (LOD) of 0.03 UNIT/ml [Figure. 4e]

which well agreed with previously reported quantitative ALP assays.[29] Additionally, the clear oxidation peak was observed within 10 minutes after addition of ALP, and the overall enzyme reaction was starting to saturate at approximately 40 minutes [Figure. S6].

After verifying the electrochemical property of graphene-Au hybrid NEAs in cell-free condition, hMSCs (2.0×10^4 cells/cm^2) that were grown on graphene-Au hybrid NEAs for a day were treated with OM. The cyclic voltammetry was conducted for differentiation period (3 weeks) with the addition of PAPP molecule [Figure. S7] for real-time monitoring of the osteogenic differentiation of hMSCs in a nondestructive manner [Figure. 4f]. We observed no obvious redox peaks on the voltammogram up to D7 even though the background signal is slightly increased. In contrast, clear, distinct redox peaks were observed in the period of the premature (D14) and mature (D21) osteoblast formation. The calculated I_{PA} values from time-dependent monitoring (range from D1 to D21) of hMSCs during osteogenic differentiation demonstrated the sequential increment of ALP activity as expected [Figure. S8]. In particular, the remarkable signal increment was observed from D14, where premature osteoblast starts to form [Figure. 4g]. Additionally, graphene-Au hybrid NEAs also showed excellent stability by maintaining the I_{PA} value for 3 weeks under the cell-free condition [Figure. 4h].

We also analyzed for myogenic differentiation electrochemically at D21 [Figure. S9] to show that our graphene-Au hybrid NEAs could discriminate osteogenic differentiation from other types of differentiation. Compared to hMSCs, myoblast cell also demonstrated higher ALP activity;[30] however, osteoblasts expressed approximately 2 times higher signals (ΔI_{PA}: −1.80 μA) relative to myoblasts (ΔI_{PA}: −0.82 μA) which showed the ability of graphene-Au hybrid NEAs to discriminate osteogenic differentiation from other differentiation. Supportably, cell destructive a PNPP based optical ALP assay also demonstrated similar trends on ALP activity of each cell line (undifferentiated hMSC, osteoblast, and myoblast) observed by graphene-Au hybrid NEAs. Thus, we believe that our graphene-Au hybrid NEAs will be particularly valuable for enhancing and monitoring stem cell behaviors through unique biophysical and electrochemical properties. The non-destructive, real-time monitoring of stem cell differentiation would be valuable for the clinical application of stem cell therapies to repair the damaged tissue/organs of patients.

In summary, we have successfully developed multifunctional graphene-gold (Au) hybrid nanoelectrode arrays (NEAs) for modulating the extent of osteogenic differentiation of stem cells. Potentially, our developed approach can be beneficial for deconvoluting biophysical cues from the complex microenvironmental cues and identify the combinatorial cues to enhance stem cell differentiation. More detailed mechanistic studies on how the combination of physicochemical and biophysical cues modulate the signaling cascades involved in stem cell osteogenesis are currently under investigation. Furthermore, due to the excellent biocompatibility and electrochemical performance of our hybrid NEAs, the osteogenic differentiation of hMSCs was successfully monitored in both non-destructive and real-time manner. Since the destructive analysis process such as cell lysis and cell fixation are not necessary for assaying the osteogenic differentiation of hMSCs for transplantation, our developed combinatorial arrays and novel electrochemical detection method can bring a breakthrough in the preclinical investigation of differentiated osteoblasts. Collectively, this

work will not only advance stem cell differentiation assays by providing a practical, non-destructive, real-time monitoring tool but also help scientists understand the fundamental interactions between nanostructures and stem cells better.

Supplementary Material

Refer to Web version on PubMed Central for supplementary material.

ACKNOWLEDGEMENTS

K.B. Lee acknowledges the partial financial support from the NIH R21 (1R21AR071101–01) and New Jersey Commission on Spinal Cord (CSCR16ERG019). J.-W. Choi acknowledges the partial financial support from National Research Foundation of Korea (NRF) (2013K1A4A3055268) and (2016R1A6A1A03012845) funded by MSIP of Korea. We are also grateful to Thanapat Pongkulapa and Dr. Tae-Hyung Kim for their kind support and valuable discussion.

REFERENCES

[1]. Muller-Sieburg CE, Sieburg HB, Bernitz JM, Cattarossi G, Blood 2012, 119, 3900; [PubMed: 22408258] Cahan P, Daley GQ, Nat Rev Mol Cell Biol 2013, 14, 357; [PubMed: 23673969] Knoepfler PS, Adv Drug Deliv Rev 2015, 82–83, 192;Sterneckert JL, Reinhardt P, Scholer HR, Nat Rev Genet 2014, 15, 625. [PubMed: 25069490]

[2]. Narsinh KH, Sun N, Sanchez-Freire V, Lee AS, Almeida P, Hu S, Jan T, Wilson KD, Leong D, Rosenberg J, Yao M, Robbins RC, Wu JC, J Clin Invest 2011, 121, 1217; [PubMed: 21317531] Ben-David U, Benvenisty N, Nat Rev Cancer 2011, 11, 268. [PubMed: 21390058]

[3]. Lee AS, Tang C, Rao MS, Weissman IL, Wu JC, Nat Med 2013, 19, 998; [PubMed: 23921754] Knoepfler PS, Stem Cells 2009, 27, 1050. [PubMed: 19415771]

[4]. Dalby MJ, Gadegaard N, Oreffo RO, Nat Mater 2014, 13, 558. [PubMed: 24845995]

[5]. Kilian KA, Bugarija B, Lahn BT, Mrksich M, Proc Natl Acad Sci U S A 2010, 107, 4872; [PubMed: 20194780] Wang X, Li S, Yan C, Liu P, Ding J, Nano Lett 2015, 15, 1457. [PubMed: 25697623]

[6]. Lee WC, Lim CH, Shi H, Tang LA, Wang Y, Lim CT, Loh KP, ACS Nano 2011, 5, 7334. [PubMed: 21793541]

[7]. McBeath R, Pirone DM, Nelson CM, Bhadriraju K, Chen CS, Dev Cell 2004, 6, 483; [PubMed: 15068789] Tsui JH, Janebodin K, Ieronimakis N, Yama DMP, Yang HS, Chavanachat R, Hays AL, Lee H, Reyes M, Kim DH, ACS Nano 2017, 11, 11954. [PubMed: 29156133]

[8]. Nayak TR, Andersen H, Makam VS, Khaw C, Bae S, Xu X, Ee PL, Ahn JH, Hong BH, Pastorin G, Ozyilmaz B, ACS Nano 2011, 5, 4670. [PubMed: 21528849]

[9]. Yang J, McNamara LE, Gadegaard N, Alakpa EV, Burgess KV, Meek RM, Dalby MJ, ACS Nano 2014, 8, 9941. [PubMed: 25227207]

[10]. Goodwin HS, Bicknese AR, Chien SN, Bogucki BD, Quinn CO, Wall DA, Biol Blood Marrow Transplant 2001, 7, 581; [PubMed: 11760145] Kim TH, Yea CH, Chueng ST, Yin PT, Conley B, Dardir K, Pak Y, Jung GY, Choi JW, Lee KB, Adv Mater 2015, 27, 6356. [PubMed: 26390254]

[11]. Pittenger MF, Mackay AM, Beck SC, Jaiswal RK, Douglas R, Mosca JD, Moorman MA, Simonetti DW, Craig S, Marshak DR, Science 1999, 284, 143; [PubMed: 10102814] Tsimbouri PM, Childs PG, Pemberton GD, Yang J, Jayawarna V, Orapiriyakul W, Burgess K, González-García C, Blackburn G, Thomas D, Vallejo-Giraldo C, Biggs MJP, Curtis ASG, Salmerón-Sánchez M, Reid S, Dalby MJ, Nature Biomedical Engineering 2017, 1, 758;Kanczler JM, Oreffo RO, Eur Cell Mater 2008, 15, 100. [PubMed: 18454418]

[12]. Lutolf MP, Gilbert PM, Blau HM, Nature 2009, 462, 433; [PubMed: 19940913] Chen W, Shao Y, Li X, Zhao G, Fu J, Nano Today 2014, 9, 759; [PubMed: 25883674] Iskratsch T, Wolfenson H, Sheetz MP, Nat Rev Mol Cell Biol 2014, 15, 825; [PubMed: 25355507] Murphy WL, McDevitt TC, Engler AJ, Nat Mater 2014, 13, 547. [PubMed: 24845994]

[13]. Chen D, Feng H, Li J, Chem Rev 2012, 112, 6027; [PubMed: 22889102] Zhou M, Zhai Y, Dong S, Anal Chem 2009, 81, 5603. [PubMed: 19522529]

[14]. Lee JH, Oh BK, Choi JW, Biosens Bioelectron 2013, 49, 531. [PubMed: 23816850]

[15]. Engler AJ, Sen S, Sweeney HL, Discher DE, Cell 2006, 126, 677. [PubMed: 16923388]

[16]. Kim KS, Jeong H, Jeong MS, Jung GY, Advanced Functional Materials 2010, 20, 3055.

[17]. Selhuber-Unkel C, Lopez-Garcia M, Kessler H, Spatz JP, Biophys J 2008, 95, 5424. [PubMed: 18689459]

[18]. Kim TH, Shah S, Yang L, Yin PT, Hossain MK, Conley B, Choi JW, Lee KB, ACS Nano 2015, 9, 3780; [PubMed: 25840606] Li X, Choy WCH, Ren X, Zhang D, Lu H, Advanced Functional Materials 2014, 24, 3114;Yi N, Zhang C, Song Q, Xiao S, Sci Rep 2016, 6, 25134. [PubMed: 27118247]

[19]. Stankovich S, Dikin DA, Piner RD, Kohlhaas KA, Kleinhammes A, Jia Y, Wu Y, Nguyen ST, Ruoff RS, Carbon 2007, 45, 1558;Eigler S, Dotzer C, Hirsch A, Carbon 2012, 50, 3666.

[20]. You MH, Kwak MK, Kim DH, Kim K, Levchenko A, Kim DY, Suh KY, Biomacromolecules 2010, 11, 1856. [PubMed: 20568737]

[21]. Khetan S, Guvendiren M, Legant WR, Cohen DM, Chen CS, Burdick JA, Nat Mater 2013, 12, 458. [PubMed: 23524375]

[22]. Geiger B, Bershadsky A, Curr Opin Cell Biol 2001, 13, 584. [PubMed: 11544027]

[23]. Chen Q, Shou P, Zheng C, Jiang M, Cao G, Yang Q, Cao J, Xie N, Velletri T, Zhang X, Xu C, Zhang L, Yang H, Hou J, Wang Y, Shi Y, Cell Death Differ 2016, 23, 1128; [PubMed: 26868907] Ge C, Yang Q, Zhao G, Yu H, Kirkwood KL, Franceschi RT, J Bone Miner Res 2012, 27, 538. [PubMed: 22072425]

[24]. Wang J, Electroanalysis 2005, 17, 7;Yu AM, Liang ZJ, Cho J, Caruso F, Nano Letters 2003, 3, 1203.

[25]. Fu YS, Ji SH, Chen X, Ma XC, Wu R, Wang CC, Duan WH, Qiu XH, Sun B, Zhang P, Jia JF, Xue QK, Phys Rev Lett 2007, 99, 256601; [PubMed: 18233541] Zhu C, Yang G, Li H, Du D, Lin Y, Anal Chem 2015, 87, 230. [PubMed: 25354297]

[26]. Ambrosi A, Chua CK, Bonanni A, Pumera M, Chem Rev 2014, 114, 7150. [PubMed: 24895834]

[27]. Beresford JN, Bennett JH, Devlin C, Leboy PS, Owen ME, J Cell Sci 1992, 102, 341; [PubMed: 1400636] Beck GR, Sullivan EC, Moran E, Zerler B, J Cell Biochem 1998, 68, 269. [PubMed: 9443082]

[28]. Balis N, Stratakis E, Kymakis E, Materials Today 2016, 19, 580;Yeo J-S, Kang R, Lee S, Jeon Y-J, Myoung N, Lee C-L, Kim D-Y, Yun J-M, Seo Y-H, Kim S-S, Nano Energy 2015, 12, 96.

[29]. Jiao H, Chen J, Li W, Wang F, Zhou H, Li Y, Yu C, ACS Appl Mater Interfaces 2014, 6, 1979. [PubMed: 24417549]

[30]. Safadi A, Livne E, Silbermann M, Reznick AZ, J Histochem Cytochem 1991, 39, 199; [PubMed: 1987264] Dellavalle A, Sampaolesi M, Tonlorenzi R, Tagliafico E, Sacchetti B, Perani L, Innocenzi A, Galvez BG, Messina G, Morosetti R, Li S, Belicchi M, Peretti G, Chamberlain JS, Wright WE, Torrente Y, Ferrari S, Bianco P, Cossu G, Nat Cell Biol 2007, 9, 255. [PubMed: 17293855]

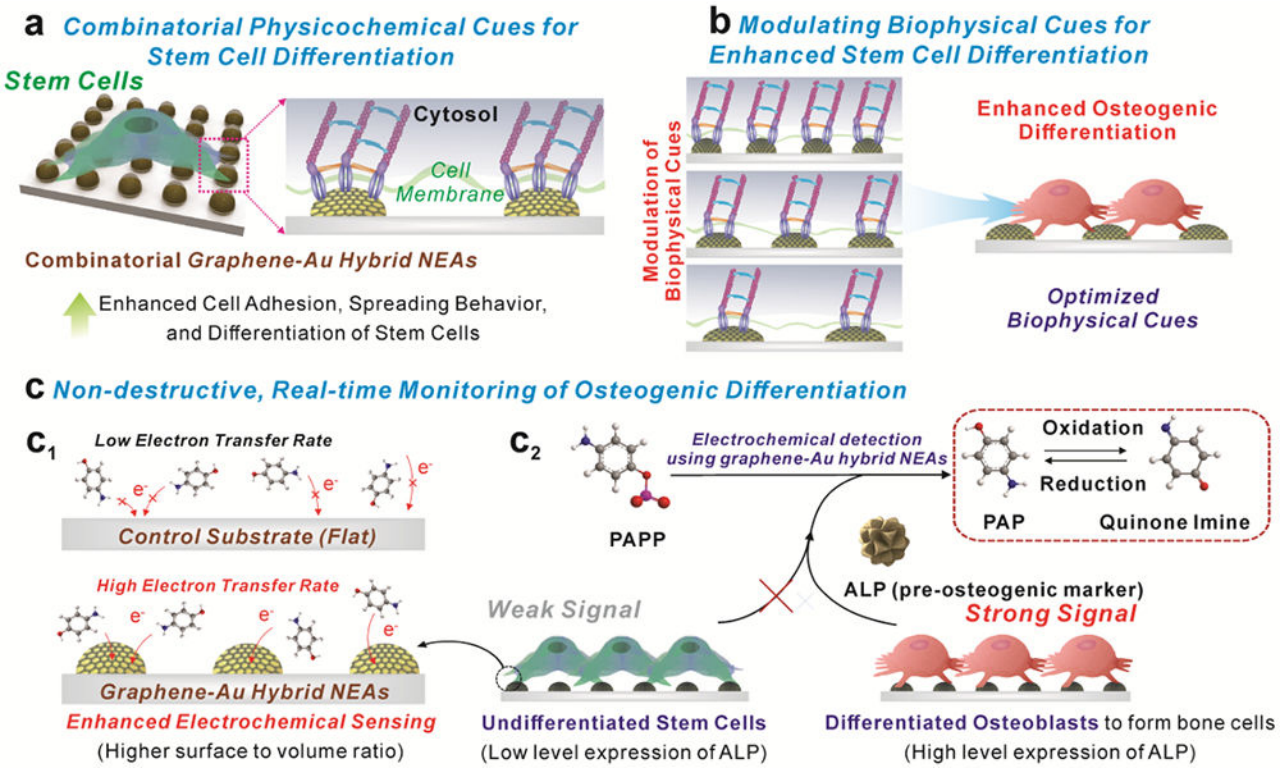

Figure 1. Schematic illustration of multifunction of graphene-Au hybrid nanoelectrode arrays (NEAs).

a) Investigation of the combinatorial effects of physicochemical cues on stem cell. **b)** Identification of optimal biophysical cues for stem cell differentiation. **c)** Enhanced electrochemical signal for monitoring osteogenic differentiation

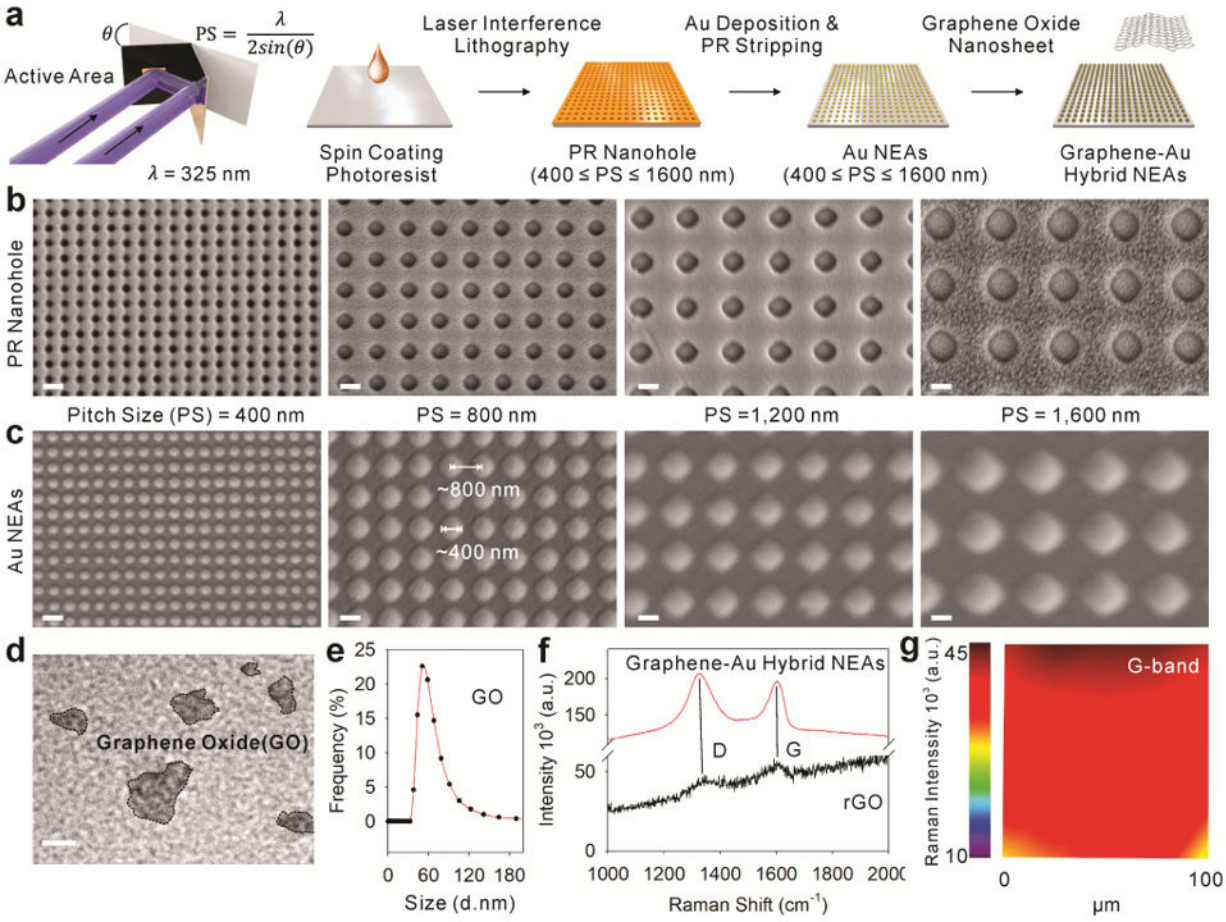

Figure 2. Generation of graphene-Au hybrid nanoelectrode arrays (NEAs).

a) Schematic illustration of sequential steps to generate graphene-Au hybrid NEAs on ITO electrode via laser interference lithography (LIL) and metal deposition method. **(b-c)** Representative scanning electron microscope (SEM) images (Magnification of 40K X) of **b)** photoresist nanohole after the LIL process and **c)** resulting Au NEAs after metal deposition process according to pitch size (400, 800, 1200, and 1600 nm, respectively). **d)** Representative transmission electron microscope (TEM) image, **e)** size distributions, and **f)** Raman spectra of synthesized graphene oxide nanosheet and after formation of graphene-Au hybrid NEAs. **g)** Homogeneity analysis by Raman map obtained from graphene-Au hybrid NEAs with notable Raman transitions band (G-band of graphene at around 1600 cm^{-1}). Scale bars are 500 nm **(b,c)** and 50 nm **(d)**.

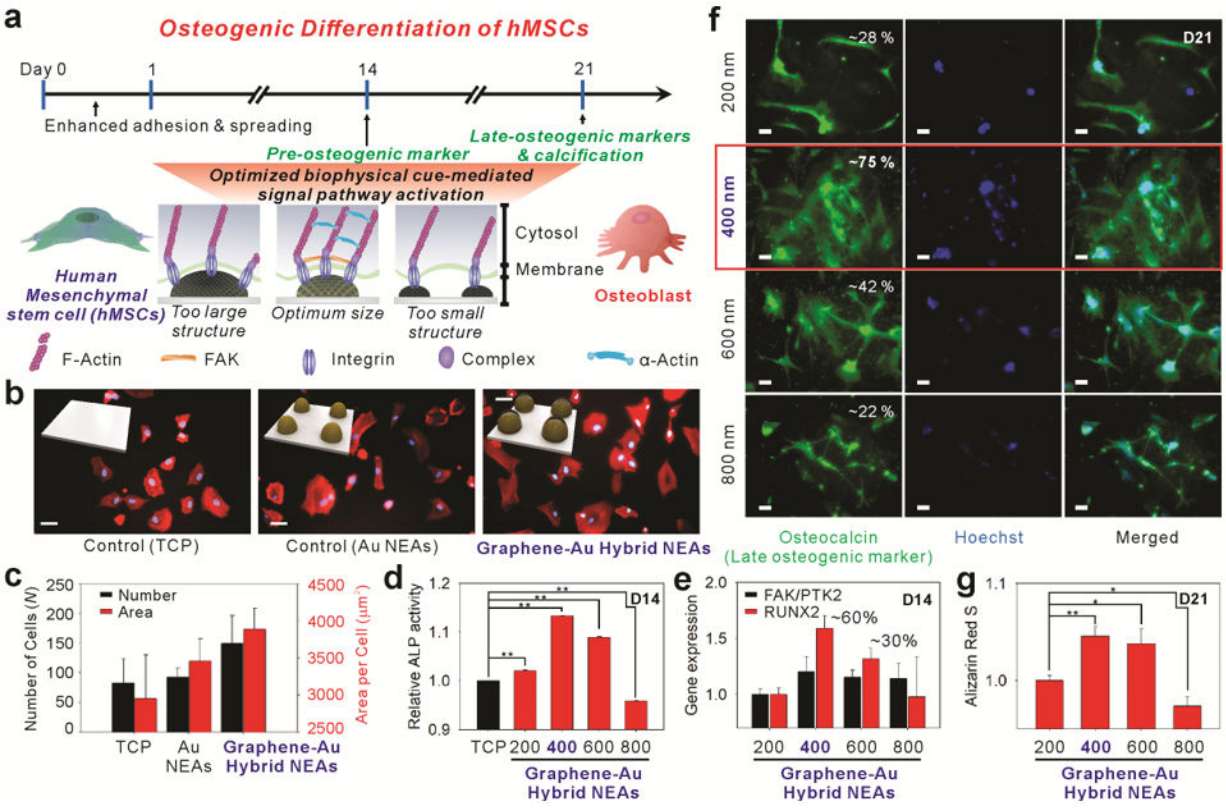

Figure 3. Enhanced osteogenic differentiation of hMSCs by graphene-Au hybrid NEAs.

a) Schematic illustration of graphene-Au hybrid NEAs effect on the osteogenic differentiation of hMSCs. **(b-c)** Analysis of cell adhesion and spreading behavior. **b)** Representative Hoechst and F-actin-stained fluorescence images of hMSCs labeled with Alexa Fluor® 633 (scale bar = 50 μm) and **c)** the calculated number of cells after washing (adhesion) and cell surface area (spreading) from F-actin-stained images of hMSCs on TCP, Au NEAs, and graphene-Au hybrid NEAs (width = 400 nm), respectively. **(d-g)** Effect of graphene-Au hybrid NEAs on osteogenic differentiation of hMSCs based on different width size range from 200 to 800 nm. **d)** Alkaline phosphatase (ALP) assay to confirm the expression of the pre-osteogenic marker based on different pitch size. **e)** PCR analysis of osteogenic markers including runt-related transcription factor 2 (RUNX2) and focal adhesion kinase (FAK) for verifying nano-topographic effect. **f)** Fluorescence images of hMSCs differentiated into osteoblasts stained for osteocalcin with Alexa 594 (red, left column), a nucleus with Hoechst (blue, middle column) and merged (right column) (scale bar = 50 μm). **g)** Quantitative analysis of calcium expression by extracting Alizarin red S based on different width size. Results are average of absorbance signals (405 and 562 nm for ALP and Alizarin red S, respectively obtained from three independent experiments) (Error bars represent mean ±s.d.; n=3, * $p < 0.05$, ** $p < 0.001$ by one-way ANOVA with Tukey post-hoc test.)

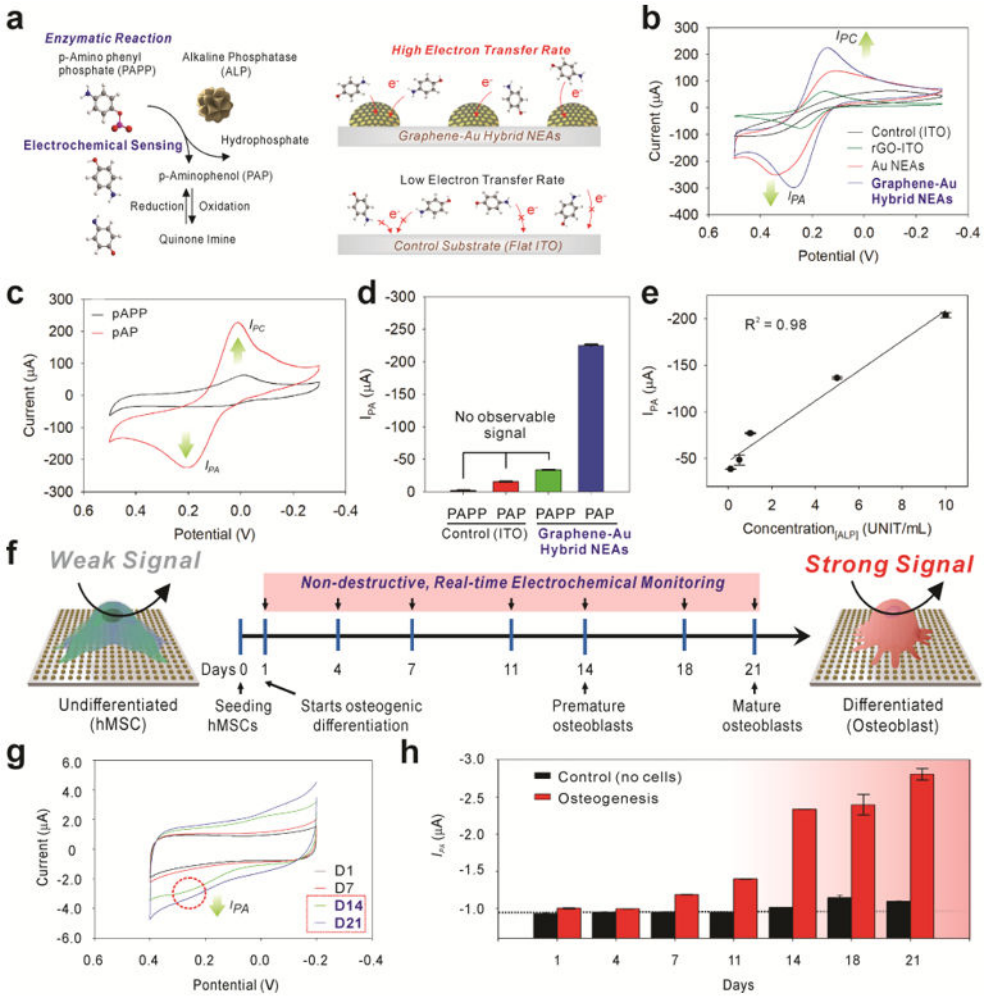

Figure 4. Utilization of graphene-Au hybrid NEAs as an electrochemical sensing platform for *in-situ* monitoring of osteogenic differentiation of hMSCs.

a) Schematic illustration of an enzymatic reaction and electrochemical sensing mechanism of alkaline phosphatase (ALP) and improved electron transfer kinetic based on the 3D surface in graphene-Au hybrid NEAs compared to 2D flat ITO surface. **b)** Cyclic voltammogram of 1 mM of $[Fe(CN)_6]^{4-}$ dissolved in DPBS obtained at a 50 mV s^{-1} scan rate using a bare ITO substrate, rGO coated ITO substrate, Au NEAs, and graphene-Au NEAs, respectively. **c)** Cyclic voltammogram of P-aminophenyl phosphate (PAPP) on graphene-Au NEAs before and after enzyme reaction with alkaline phosphatase (ALP). **d)** Anodic peak (oxidation potential: I_{PA}) value change achieved from of cyclic voltammogram of PAPP, before and after enzyme reaction (ALP), on bare ITO substrate and graphene-Au hybrid NEAs. **e)** The linear correlations between concentrations of ALP and the current signal at oxidation potential (I_{PA}) of cyclic voltammetry. **f)** Schematic illustration of electrochemical signal change between undifferentiated and differentiated (osteocyte) hMSCs based on ALP generation. **g)** Cyclic voltammetry, and **h)** calculated *Ipc* values from time-dependent monitoring (range from D1 to D21) of hMSCs during osteogenic differentiation. 8.0×10^3 cells are seeded on 0.4 cm^2 area and treated with osteogenic

differentiation medium (OM). The medium was changed after each electrochemical measurement.